Erosion Processes of the Discharge Cathode Assembly of Ring-Cusp Gridded Ion Thrusters

Alec D. Gallimore*
University of Michigan, Ann Arbor, Michigan 48109
Joshua L. Rovey[†]
Starfire Industries LLC, Champaign, Illinois 61820
and
Daniel A. Herman[‡]
QSS Group, Inc., Cleveland, Ohio 44135

An ion-thruster discharge-cathode-assembly erosion theory is presented based on near-discharge-cathode-assembly NSTAR plasma measurements and experimental results for propellant flow rate effects on ion number density. The plasma-potential structures are used in an ion-trajectory algorithm to determine the location and angle of bombarding ions at the discharge-cathode-assembly keeper. These results suggest that the plasma-potential structure causes a chamfering of the discharge-cathode-assembly keeper orifice. Results from tests with an instrumented discharge-cathode assembly show that increasing propellant flow rate causes a decrease in keeper-orifice ion number density, most likely due to charge-exchange and elastic collisions. Combining these two results, the known wear-test and extended-life-test discharge-cathode-assembly erosion profiles can be qualitatively explained. Specifically, the change in the wear profile from the discharge-cathode-assembly keeper downstream face to the keeper orifice for the extended-life test may be a result of the reduction in discharge-cathode-assembly propellant flow rate when the thruster operating point is changed from TH 15 to TH 8.

Nomenclature

E	=	energy of the incident sputtering ion
e	=	elementary charge
M_{Xe}	=	xenon mass
$\dot{m}$	=	mass flow rate
n_{ion}	=	ion number density
n_n	=	neutral number density
p	=	pressure
Y	=	sputtering yield
λ_{CEX}	=	charge-exchange mean free path
θ	=	angle of incidence relative to the target surface

I. Introduction

GRIDDED ion thrusters are high-specific-impulse, high-efficiency, advanced space propulsion systems. Three main processes compose gridded ion-thruster operation: 1) electron generation, 2) ion production through electron-bombardment ionization, and 3) ion extraction using high-voltage grids (ion optics). In modern ion thrusters, electrons are generated with a hollow cathode called the discharge cathode because it initiates and sustains the plasma discharge. Electrons from the cathode enter the discharge chamber and create ions through electron-bombardment ionization collisions with neutral atoms, typically xenon. Plasma production is enhanced by increasing the electron path length with a magnetic field. Early gridded thrusters used divergent and radial magnetic field configurations, but modern thrusters use a ring-cusp

geometry because it provides better plasma containment [1]. Ions are extracted and accelerated to significant velocity by high-voltage grids. One prominent example of a contemporary ring-cusp gridded ion thruster is the 30-cm-diam NASA solar technology and application readiness (NSTAR) ion thruster used on the Deep Space One (DS1) spacecraft.

Three wear tests performed on a 30-cm-diam thruster and the extended-life test (ELT) of the flight spare DS1 thruster have shown that extended ion-thruster operation leads to ion-bombardment sputter erosion of the discharge cathode [2–10]. During the first wear test, severe erosion of the discharge cathode was noted [4] that if left unchecked would have jeopardized the DS1 mission. A keeper electrode that is maintained at an intermediate potential between the discharge cathode and the anode was added to the discharge cathode to serve as a sacrificial shield. The combination of the discharge cathode with the keeper is called the discharge-cathode assembly (DCA). The subsequent 1000- and 8200-h wear tests showed erosion of the DCA occurring primarily from the downstream keeper face at approximately the 50% keeper radius. However, during the ELT, the primary erosion location shifted from the 50% keeper radius to the keeper orifice. This shift and an accelerated erosion rate coincided with two ELT events: a throttling down in thruster power and an inadvertent shorting event between the discharge cathode keeper and cathode common. An experimental investigation by Kolasinski and Polk [11] found evidence that the erosion location shifted when the thruster was operated at a reduced beam current condition (i.e., when the thruster was adjusted from the nominal high-power TH-15 condition to the lower-power TH-8 operating point). Nominal operating conditions for the NSTAR thruster are shown in Table 1. Note the reduction in DCA mass flow rate from TH 15 to TH 8.

A 30-cm-diam ring-cusp gridded ion thruster was used in an experimental investigation to determine and explain the physical processes responsible for DCA erosion. The investigation is divided into three main parts that correspond with the main sections of this paper. First, an experimental effort to measure thruster internal plasma properties with beam extraction is described. Second, experimental results are used to calculate the DCA erosion rate and determine the importance of doubly charged ions. Third, internal plasma properties are used to numerically simulate keeper wear

---

*Aurthur F. Thurnau Professor, Department of Aerospace Engineering. Associate Fellow AIAA.

[†]Propulsion Research Engineer. Member AIAA.

[‡]Research Engineer, Onboard Propulsion Branch. Member AIAA.

Table 1 Selected NSTAR ion-thruster nominal operating parameters

NSTAR TH level	Power level, kW	Specific impulse, s	Discharge voltage, s	Discharge current, A	Discharge-cathode mass flow, sccm of Xe	Main flow, sccm of Xe	Beam voltage, V	Beam current, A	Accel voltage, V
TH15	2.29	3120	25.14	13.13	3.70	23.43	1100	1.76	−180
TH12	1.94	3174	25.40	10.87	2.89	19.86	1100	1.49	−180
TH8	1.44	3109	25.10	8.24	2.47	14.41	1100	1.10	−180
TH4	0.97	2935	25.61	6.05	2.47	8.30	1100	0.71	−150
TH0	0.47	1972	25.20	4.29	2.47	5.98	650	0.51	−150

profiles for the TH-15 and TH-8 operating conditions. The Conclusions section summarizes the physical processes causing DCA erosion.

II. Discharge-Chamber Plasma Properties

The research presented in this paper used the FMT2 ion thruster, which is a derivative of the NSTAR ion engine. The functional model thruster (FMT) series preceded the NSTAR engineering model thrusters (EMTs), and the NSTAR flight thrusters (FTs). All three variants are based on the 30-cm-diam ring-cusp ion engine developed by NASA in the 1980s. The FMT2 has been shown to exhibit a nearly identical magnetic field topology compared with the EMTs and FTs. Furthermore, the FMT2 performance is essentially identical to that of the FTs. More detailed information on the FMT2 can be found in [12–18]. Williams [15,17] modified the FMT2 thruster to permit laser-induced fluorescence (LIF) interrogation of the discharge plasma by putting three quartz-window-covered rectangular slots into the anode wall (Fig. 1). Follow-up tests showed that these modifications did not alter the discharge-chamber magnetic field, ion production efficiency, or overall thruster performance [15–17].

Williams's [15] LIF experimental setup was further modified to allow internal electrostatic probing of the discharge plasma. The side anode quartz window is replaced by a discharge-plasma-containment mechanism permitting probe access inside the anode over a two-dimensional grid. The discharge-plasma-containment mechanism is described in detail in [12–14,19,20].

Local plasma-potential measurements are obtained using a floating emissive probe [21–23]. Electron emission from hot electrostatic probes provides a means to measure the local plasma potential directly. This measurement resolves many problems encountered with interpretation of the "knee" of the I-V potential from single Langmuir probes [24–26]. Langmuir I-V characteristics are complicated by probe geometry, magnetic fields, the presence of a flowing plasma, and ionization near the probe [22]. Emitting probes offer an alternative technique to determine the plasma potential that is less sensitive to plasma conditions.

Although plasma-potential measurements were obtained over a variety of thruster operating conditions (Table 1), only results for the TH-8 and TH-15 operating conditions will be presented here [13,19,20]. The plasma-potential contours shown in Fig. 2 for both TH 8 and TH 15 demonstrate an on-axis minimum region indicating

the plume structure of the discharge cathode. Plasma potentials inside this low-potential column are only 16 V near the discharge cathode. The potential drop is highest at the cathode orifice because the axial magnetic field is strongest there and effectively impedes the diffusion of electrons in the radial direction. The potential increase in the radial direction indicates a freestanding potential gradient that forms the transition between the discharge-cathode plume and the main discharge plasma.

Evaluation of the centerline plasma-potential values does not support the existence of a potential hill structure at the operating conditions investigated, which has been one of the proposed causes of anomalous discharge-cathode erosion [27]. Measurements internal to the DCA keeper by other researchers have also shown the absence of a potential hill [28–30]. Considering the importance of the magnetic field in shaping the discharge environment, it is not surprising that a potential hill is not present. Although the magnetic field reduces radial diffusion, the axial magnetic field enhances axial diffusion of electrons, which would tend to smooth out potential structures on the axis. This result is particularly true in regions near the discharge cathode, for which the axial magnetic field is largest.

Comparison of the two contours in Fig. 2, or of any of the plasma potentials obtained for approximately the same discharge voltage for that matter, shows negligible variations in the plasma structure at various operating conditions. It should be noted that shorting of the discharge keeper to discharge cathode common was also investigated to determine what effect the ELT keeper-shorting event had on DCA erosion. Perhaps not surprisingly, keeper shorting did not have a significant effect on the near-DCA plasma structure outside of the keeper sheath [13,19].

A closer look at the near-DCA plasma contours (Fig. 3) for both TH 8 and TH 15 highlights an important finding: the high-density, low-plasma-potential plume structure is distinctly different from the bulk discharge plasma. Large radial potential gradients exist because of the largely axial magnetic field topology near the DCA. This freestanding gradient structure is termed a double layer. Double layers form the transition between two plasmas that are at two different potentials. A double layer forms the boundary between the discharge-cathode plume and the bulk discharge plasma [31–33]. The magnetic field, potential gradients, and double layer are all tied together. The magnetic field reduces radial electron motion, creating the potential gradient in the radial direction and the high-density plume along the centerline.
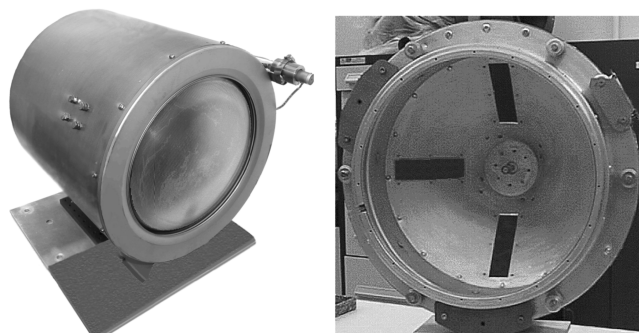
Fig. 1 FMT2 thruster (left) and FMT2 discharge chamber illustrating rectangular slots (right).
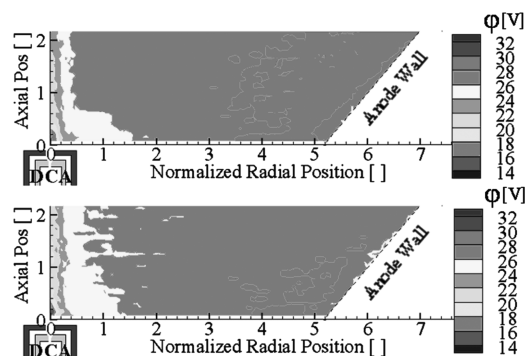
Fig. 2 FMT2 floating emissive probe plasma-potential contours for TH 8 (top) and TH 15 (bottom).
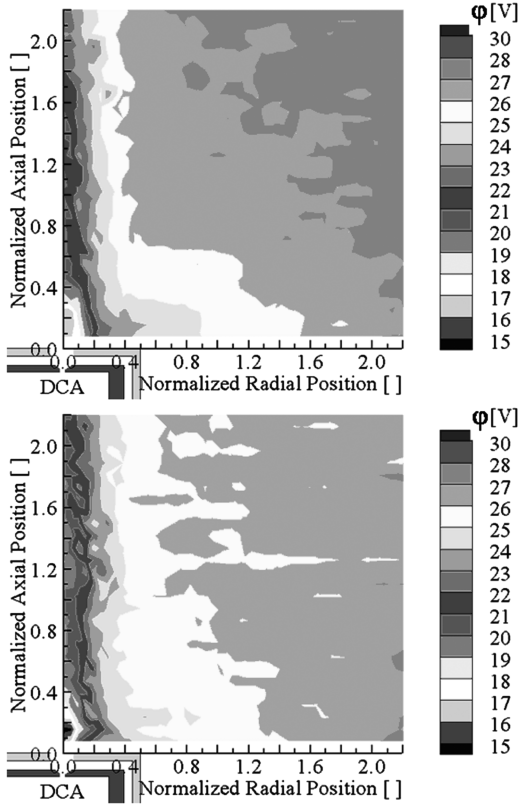
Fig. 3 Near-discharge-cathode-assembly FMT2 floating emissive probe plasma-potential contours for TH 8 (top) and TH 15 (bottom).

Near the cathode keeper, there is a potential difference of approximately 10 V across the double layer, which roughly spans the length from the cathode centerline to the discharge-keeper plate radius. The difference in cathode-keeper and cathode-common potential is 5–7 V for these operating conditions. Combining the potential drop through the discharge plasma with a nonshorted keeper-sheath fall yields an accelerating potential of approximately 20–21 V.

III.   DCA Erosion-Rate Calculations

The application of the measured plasma potentials to calculate DCA erosion rates is difficult due to the lack of an accurate low-energy, heavy-ion, sputter-yield description. Recently, experimental data taken by Doerner et al. [34,35] reported sputter-yield data for Xe^+–Mo with ion-bombardment energies from 10 to 200 eV. The spectroscopic sputter yields and standard weight loss yields calculated by Doerner compare nicely with each other and with existing low-energy Xe^+–Mo data taken by other researchers, thus validating the Doerner et al. results. A sixth-order polynomial fit was made to a log–log plot of the Doerner et al. sputter-yield versus energy data. From this fit, an empirical determination of the normal incident sputtering yield of the low-energy Xe^+–Mo system is determined as a function of energy [Eq. (1)]. The Doerner et al. [35] results indicate a normal threshold energy of ~15 eV for xenon sputtering of molybdenum.

$$
\begin{aligned}
Y_{\text{Doerner}}(E) = \exp\{ & -0.372304[\ell_n(E)]^6 + 9.48041[\ell_n(E)]^5 \\
& - 100.046[\ell_n(E)] + 560.276[\ell_n(E)]^3 - 1758.24[\ell_n(E)]^2 \\
& + 2940.48[\ell_n(E)] - 2064.3 \}
\end{aligned}
\tag{1}
$$

In Eq. (1), Y is the sputtering yield and E is the energy of the incident sputtering ion. Numerous investigations have shown that sputtering yields have an angular dependence [36–41]. Yamamura's [37] empirical formula for the angular dependence of sputtering, specifically for the low-energy Xe^+–Mo system, is given as [42]

$$
\left(\frac{Y(\theta)}{Y(0)}\right) = \cos^{-19.96}\theta \cdot \exp[-13.55(\cos^{-1}\theta - 1)]
\tag{2}
$$

In Eq. (2), the numeric factors are energy-dependent fit parameters determined from 100-eV xenon ions impacting a molybdenum target, $Y(0)$ is the sputtering yield at normal incidence, and θ is the angle of incidence relative to the target surface [42]. The exponent fit parameter, 19.96, carries the threshold effect and is a function of the ratio E/E_{th}. Yamamura's formula will be used over other formulas because it is based upon low-energy data as opposed to empirical formulas that are generic to multiple incident particle-target systems and/or rely heavily on extrapolation from high-energy data. Combining Eqs. (1) and (2), the sputtering yield as a function of incident particle energy and angle is determined. The minimum threshold energy as a function of incident angle for the Xe^+–Mo system is 8 eV, which occurs at 48 deg.

Two additional pieces of information are required before an erosion-rate calculation based on measured plasma potentials can be made: the incoming particle angle of incidence and the number of particles impacting the keeper face. Based upon LIF-measured ion velocities in the FMT2 discharge chamber, an incident presheath angle of approximately 60 deg (with respect to the keeper normal) is most likely [15–18].

The ion is assumed to be accelerated through the sheath normal to the surface by the potential difference between the presheath potential of 22 V and the discharge-keeper floating potential (5–7 V). The through-sheath energy and angle are calculated, giving the incident ion energy with angular dependence. The effect of shorting the cathode keeper to cathode common can also be investigated by reducing the keeper floating potential to 0 V.

The number of incident ions can be estimated from the number-density measurements made over the same spatial domain as the plasma-potential measurements. Ion number densities are measured with a Langmuir probe using a thin-sheath analysis with a sheath-thickness-correction algorithm [13,14,19]. The ion number density just outside the double layer, approximately a keeper radius from the cathode centerline and in the plane of the keeper face in the radial and axial directions, is roughly 5×10^{11} cm^{-3} [13,19]. The flux of ions toward the keeper is assumed to be a directed drift with an energy corresponding to the fall voltage, given next:

$$
n_{\text{ion}} \sqrt{\frac{2e(\phi_p - \phi_{\text{CK}})}{M_{Xe}}}
\tag{3}
$$

In Eq. (3), $(\phi_P - f_{\text{CK}})$ is the difference in potentials between the plasma outside the double layer and the discharge-cathode-keeper floating potential. The keeper erosion rate is then calculated as the yield from Doerner's data fit as a function of incident energy and angle multiplied by the ion flux times the number density of the molybdenum target. The calculated erosion rates for TH 15 with only singly ionized xenon are 8 and 49 μm/kh for the cathode-keeper floating and shorted to common, respectively [19]. Because plasma potentials are roughly equivalent for TH-8 and TH-15 conditions, erosion rates are similar. The measured erosion rates for the 1000- and 8200-h NSTAR wear tests were 70 and 63 μm/kh, respectively [2,5–7]. The first 5850 h of the ELT had an estimated erosion rate of 77 μm/kh and an estimated accelerated rate of 173 μm/kh after the shorting event and throttling down to TH 8 [9,10,19,43,43,44]. The erosion rates calculated from the measured plasma parameters, assuming only singly ionized xenon, are considerably less than the measured wear-test erosion rates, which indicates that the analysis has not accurately accounted for all of the dominant factors in DCA erosion.

It appears as though the shorting event of the ELT did significantly contribute to the increased erosion observed in this wear test. The effect of shorting the discharge cathode keeper to cathode common does have a significant effect on the calculated erosion rates, resulting in an increase of roughly a factor of 6 for the conditions investigated.

A major simplification in the preceding erosion calculation is that it does not account for the increased erosion caused by doubly ionized xenon. The ratio of the double-to-single-ion-current ratio near the DCA is unknown. Traditionally, the measured double-to-single-ion currents in the plume have been used to estimate the double-to-single-number-density ratio inside the engine. A range of values has been measured in the plume of the NSTAR thruster for the double-to-single-ion current: 0.02–0.34 [45–47]. A doubly charged ion would carry a charge of twice the singly ionized xenon ion and would therefore be accelerated to twice the energy for a given electric field. The double-to-single-current ratio is converted to a number density for each species by taking into account both that the double-ion-current accounts for each double ion twice and the dependence of ion velocity with charge state, assuming constant accelerating potentials. A fixed double-to-single-number-density ratio of 0.20 is used in this analysis because it is consistent with measured values in the plume at the high-power range of the NSTAR throttling table [47]. Although this value is on the high end of the double-to-single-ion ratio measured in the plume, this value is likely to be representative of the plasma state near the DCA, given the proximity to the ionization source.

When the doubly charged ions are accounted for, the calculated erosion-rate increases as expected. For a double-to-single ratio of 0.20, the measured total ion number density of 5×10^{11} cm^{-3}, and a local plasma potential of 27 V outside the double layer, the calculated erosion rate is 54 μm/kh for the standard keeper voltage and 165 μm/kh when the keeper is shorted to the cathode [19]. These new values are close to the ELT estimated erosion rates noted earlier and suggest that the keeper shorting, in combination with the presence of doubly charged xenon ions, contributed significantly to the large DCA erosion observed in the ELT.

It follows from the preceding erosion calculation that because only the number densities increase slightly as the engine is throttled to higher power and the plasma-potential mappings depend primarily on discharge voltage only, the erosion rate is expected to increase slightly as the engine is throttled to higher power. There is no reason to expect, based upon this erosion analysis alone, that TH 8 would result in an increased erosion rate compared with TH 15. Therefore, additional factors must account for the observed ELT DCA erosion pattern.

IV. Keeper Wear Profiles

The plasma-potential results for TH 15 and TH 8 (Figs. 2 and 3) are coupled with an erosion-rate calculation to numerically simulate keeper wear. Flow rate effects are then incorporated to qualitatively predict wear profiles for TH 15 and TH 8.

A. Ion-Trajectory Calculation

An ion-trajectory calculation is used to determine the bombarding-ion impact angle, energy, and location at the keeper downstream face. The trajectory simulation procedure consists of five main steps:

1) Load the plasma-potential maps of the 30-cm thruster described earlier.

2) Calculate the electric field produced by the variation of plasma potential with spatial location.

3) Determine initial conditions for a simulation ion.

4) Iteratively calculate the ion trajectory based on the initial conditions.

5) Determine if the ion impacts the keeper and, if so, at what impact location, energy, and angle.

Because the TH-8 and TH-15 throttle points are of primary importance for comparison with the ELT, keeper wear profiles are simulated only for these two conditions. The experimental plasma-potential measurements are interpolated onto a 1 by 1-mm grid such that the entire computational domain has 4400 grid points. The electric field is calculated by using the plasma potential at the six adjacent grid points.

Table 2 shows the ion initial conditions investigated. A single simulation has 35,200 ions with 4400 initial positions (an ion starts from each of the computational domain grid points) and 8 initial

Table 2 Ion initial conditions

Locations	4400 points ($\Delta x = 1.0$ mm)
Charge state	Single, doubly
Initial energy (velocity), eV	Warm 5 eV and cold 0.05 eV
Angular orientation, deg	0, 45, 90, 135, 180, 225, 270, 315

angular orientations. Angular orientations of 0 and 90 deg correspond to an initial velocity in the radial and axial directions, respectively. Simulations are completed for both warm and cold ions, as well as singly and doubly charged ions. Warm and cold ions are assumed to have initial energies of 5 and 0.05 eV, respectively [46].
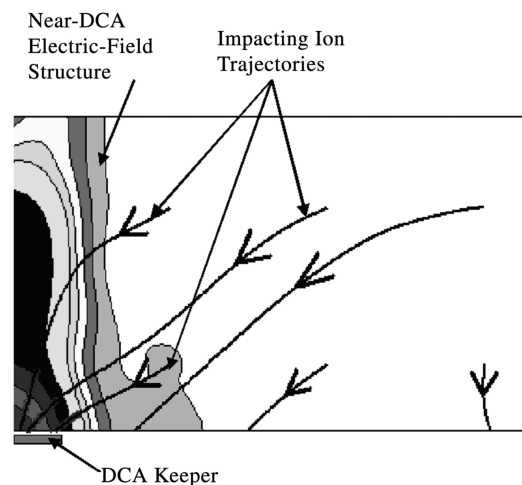
Starting with the initial conditions, an ion trajectory is calculated by iterating through the Lorentz force equation. For the simulations presented here, the magnetic field inside the ion thruster is assumed to have a negligible impact on ion motion. This assumption is justified because the ion cyclotron radius is significantly larger than the thruster dimensions. The trajectory calculation iterative procedure loop is as follows:

1) Interpolate the electric field at the ion position.

2) Calculate the new velocity components.

3) Determine the new spatial location by assuming the new velocity components are constant over the time step.
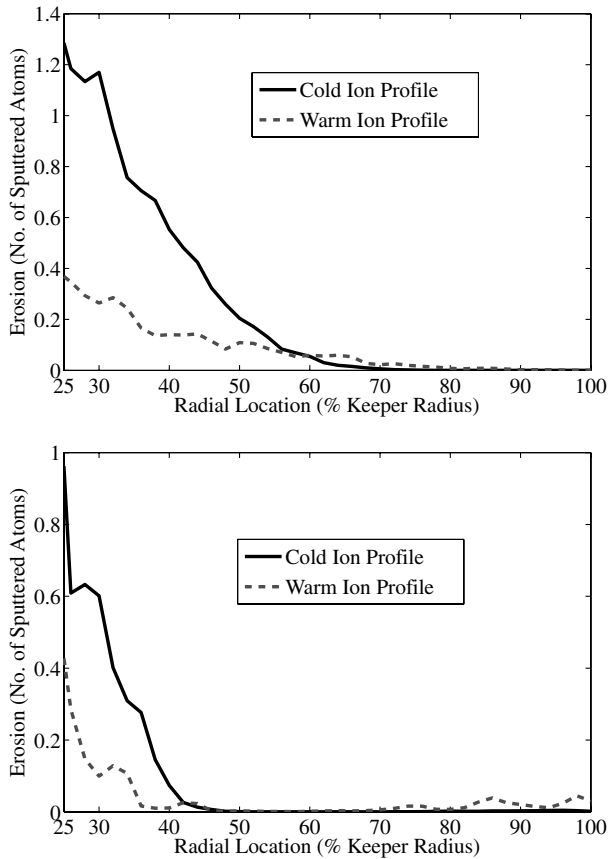
4) Repeat.

This procedure loop is iterated until the ion exits the computational domain. If the ion exit position is at the DCA keeper, then the ion location and velocity are recorded and the bombarding angle is calculated. These computations calculate the presheath angle, presheath velocity, and presheath location of each ion. Examples of ion trajectories through the calculated electric-field profile are shown in Fig. 4. Note that three of the six ions impact the keeper.

B. Erosion Calculation

Ions first pass through the keeper sheath before impacting, and so the through-sheath impact location, angle, and energy must be determined. An ion is assumed to translate only axially through the sheath. Therefore, the through-sheath impact location is equivalent to the presheath location. This assumption is justified by the small thickness of the sheath and the small radial electric fields expected within the sheath. The presheath radial velocity is assumed constant through the sheath and the axial velocity component is assumed to increase correspondingly with the gain in energy through the keeper-sheath potential drop. The angle of the vectoral sum of these two velocity components constitutes the through-sheath impact angle. The measured near-DCA plasma potential ($\sim$14 V) minus the floating keeper potential ($\sim$5 V) determines the keeper-sheath potential drop of $\sim$9 V. The bombarding-ion energy is calculated as the ion kinetic energy using the through-sheath velocity components.

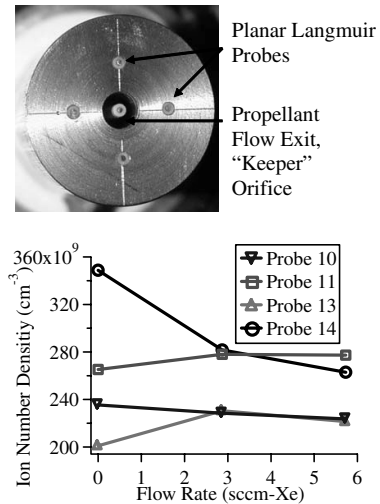Fig. 4 Example ion trajectories through the calculated electric-field profile.

Fig. 6   Instrumented dormant cathode (top) and ion number density as a function of propellant flow rate (bottom). Note the orifice probe (probe 14) and 50% keeper-radius probes.

D.   Propellant Flow Rate Effects

A multiple-cathode discharge-chamber (MCDC) [48,49] ion thruster was used to predict the effects of propellant flow rate on near-DCA plasma properties. The MCDC is a rectangular discharge chamber designed to increase gridded ion-thruster operational lifetime by operating three DCAs sequentially. Therefore, at any time, the MCDC contains an active DCA and two dormant cathodes. An experimental investigation with the MCDC studied the effect of propellant flow rate on plasma properties near the dormant cathode orifice. The dormant cathode appears similar to the DCA, but is outfitted with five planar Langmuir probes (Fig. 6). One probe is located in the dormant cathode orifice and the other four are spaced symmetrically about the centerline at the 50% keeper radius.

Results reported in Fig. 6 are for the probe located in the keeper orifice (probe 14) and the probes located at the 50% keeper-radius location. Similar results are obtained for different MCDC operating configurations. The number density at the orifice decreases by approximately 25% when the propellant flow is adjusted from zero to the full DCA flow rate (5.73 sccm). However, the ion number density at the 50% keeper radius is relatively unaffected. These results suggest that propellant flow through the dormant cathode may be shielding the orifice from bombarding ions through elastic and charge-exchange (CEX) collisions, in which the latter are known to cause changes in near-DCA ion-energy distributions when a gas flow is present [50].

Further verification of the presence of CEX collisions at the DCA orifice is obtained by evaluating the CEX mean free path (MFP). Assuming the neutral temperature at the DCA keeper orifice is 1000 K [51] and the velocity is equal to the sound speed, the keeper-orifice neutral pressure is calculated using the conservation of mass. If the bombarding ions are assumed to have a kinetic energy equal to the plasma potential ($\sim$27 V), then the CEX collision cross section is equal to 45 Å^2 [52,53] and the CEX MFP is 1.5 and 1.0 mm for the TH-8 and TH-15 operating conditions, respectively. These results are summarized in Table 3. Because the CEX MFP is the same order of magnitude as the keeper-orifice diameter, these results suggest that

Fig. 5   Simulated erosion profiles for the warm- and cold-ion assumptions for TH-15 (top) and TH-8 NSTAR (bottom) plasma-potential maps.

Using the through-sheath impact angle and energy, the number of sputtered atoms for each incident ion is calculated with Eqs. (1) and (2). Summing over all the ions that impact the keeper provides the number of sputtered atoms as a function of radial location on the keeper faceplate, which yields the simulated keeper wear profiles discussed next.

C.   Simulated Keeper-Wear-Profile Results

Figure 5 shows simulated keeper wear profiles for the warm (5 eV) and cold-ion (0.05 eV) assumptions for the TH-15 and TH-8 thruster operating conditions. Doubly charged ions tend to increase the magnitude of the profile, but have no effect on the shape. The warm-ion assumption results in less erosion of the keeper than with the cold ions, because higher-energy ions are capable of escaping from the near-DCA low-plasma-potential region, whereas less energetic cold ions are more easily pulled into the keeper by the potential field. Because Williams [15] measured ion temperatures of 0.75 eV in the near-DCA discharge-chamber plasma of the FMT2, the true erosion profile is assumed to be closer to the cold-ion results.

Both the TH-15 and TH-8 results predict an erosion profile that leads to chamfering of the keeper orifice. The increase in erosion at the keeper orifice ($\sim$25% keeper radius) leads to a chamfering profile that causes the orifice diameter to increase until the entire keeper face is eroded. This analysis suggests that the plasma-potential structure causes the primary erosion location to be at the DCA keeper orifice. However, results from the 1000- and 8200-h wear tests show the dominant erosion location to be at the 50% keeper-radius location. Furthermore, Kolasinski and Polk [11] showed that the primary erosion location shifts from the 50% radius to the orifice when thruster operation is adjusted from TH 15 to TH 8. Therefore, based on the simulated keeper-wear-profile results, the near-DCA plasma-potential structure alone cannot be causing the known erosion results.

Table 3   NSTAR DCA keeper-orifice neutral pressure, number density, and CEX MFP calculation results

Operating Condition	TH 8	TH 15
$\dot{m}$ (mg/s)	0.24	0.36
p, Pa	14.9	22.3
p, mtorr	111.8	167.3
n_n, m^{-3}	1.1×10^{21}	1.6×10^{21}
λ_{CEX}, mm	1.5	1.0
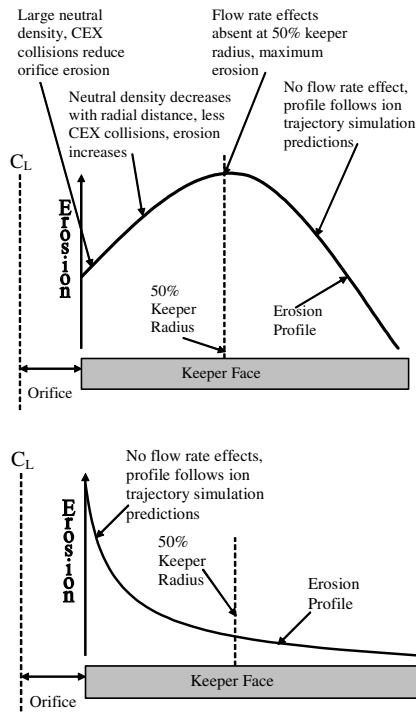
Fig. 7   Qualitative erosion profile predictions for TH 15 (top) and TH 8 (bottom).
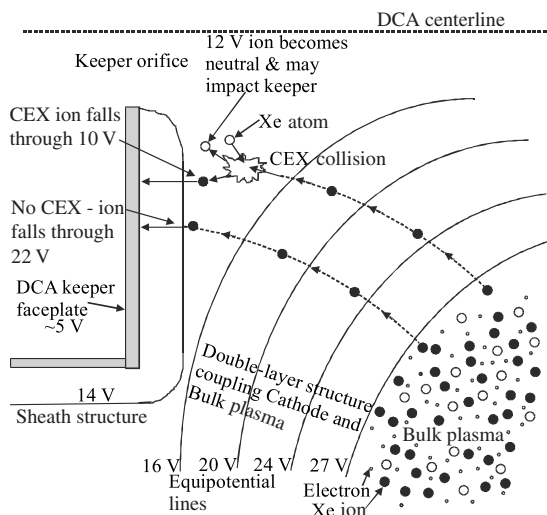
Fig. 8   Schematic illustrating the DCA erosion processes. The double-layer structure coupling the bulk and cathode plasma pulls and focuses ions into the DCA. CEX collisions reduce ion bombarding energy.

CEX collisions are occurring near the orifice, with a smaller CEX MFP and therefore more CEX collisions, during operation at TH 15.

E.   TH-15 and TH-8 Qualitative Wear Profiles

Keeper wear profiles are qualitatively predicted by combining the trends obtained with the simulation results from Fig. 5 and the propellant flow rate effects highlighted in Fig. 6. TH 15 is the high-power, higher-flow-rate condition (Table 1). Figure 7 shows the predicted erosion profile for TH 15. Near the DCA keeper orifice, the bombarding-ion number density and bombarding energy are reduced due to CEX collisions with expelled neutral propellant. As the radial distance from the orifice increases, the neutral density and corresponding number of CEX collisions decreases, leading to an increase in erosion. At approximately 50% keeper radius, the effects of propellant flow rate are no longer present. Therefore, the 50% keeper radius corresponds to the maximum erosion point. At larger

radial locations, the erosion profile corresponds with the wear-profile simulation results that exclude propellant flow effects.

The TH-8 operating point uses less DCA propellant flow than TH 15 (0.24 vs 0.36 mg/s). The reduction in DCA flow rate reduces the keeper-orifice neutral density and, therefore, the ability of the DCA orifice to protect itself from bombarding ions through CEX collisions. The TH-8 erosion profile is identical to the wear profiles predicted by these simulations (Fig. 7).

V.   Conclusions

Based on the results from the presented investigation, this section describes conclusions regarding the physical processes responsible for DCA erosion in ring-cusp gridded ion thrusters. Figure 8 illustrates the physical erosion processes.

The double-layer plasma-potential structure that couples the bulk and cathode plasmas focuses and drives ions toward the DCA. Some bombarding ions suffer CEX collisions with the neutral xenon atoms being expelled from the DCA, the products of which include a "slow" CEX ion and a "fast" neutral. The CEX ion is easily pulled toward the DCA keeper by the ambient electric field. However, CEX ions are created at a lower potential than ions originating in the bulk plasma and therefore have a significantly lower bombarding energy ($\sim$10 V instead of $\sim$22 V for Xe$^+$). Focusing on the Xe$^+$ case, the neutral xenon particle resulting from the CEX collision may also impact the keeper and cause erosion. However, the neutral is not accelerated through the plasma-potential structure and therefore impacts the keeper with the pre-CEX ion energy ($\sim$12 V). Therefore, the presence of CEX collisions decreases keeper erosion because a single high-energy bombarding ion from the bulk plasma ($\sim$22 V) is substituted with two lower-energy particles: a CEX ion ($\sim$10 V) and a neutral atom ($\sim$12 V). Each of the two resulting particles has lower energy than the initial ion and causes less erosion. In fact, the energy of each of the post-CEX particles may be lower than the threshold energy of the target material, in which case, no sputtering erosion occurs.

The presence of doubly charged ions and the effect of shorting the keeper to common both have a significant effect on the DCA erosion rate. A double-to-single-plume-current ratio of 0.25 was measured in ion-thruster plumes and the incorporation of doubles in the erosion calculation yields erosion rates that are consistent with the NSTAR wear-test data. Particularly, the ELT erosion rate before and after shorting of the keeper to common are consistent with the predicted values.

The DCA erosion processes explain the ELT results and those presented by Kolasinski and Polk [11] that show the primary erosion location shifting from the 50% keeper radius to the keeper orifice when thruster operation is changed from TH 15 to TH 8. At the onset of the ELT the thruster is operated at TH 15 and it suffers erosion at the 50% keeper radius on the keeper downstream face (TH-15 erosion profile, Fig. 7). At $\sim$4500 h into the test, the thruster is adjusted to the lower-power lower-flow-rate TH-8 operating point, which causes the erosion profile to shift due to the change in DCA flow rate. As such, erosion now occurs at the keeper orifice, leading to a chamfering profile (Fig. 7). The cathode-to-keeper short at $\sim$6400 h only increases the erosion rate; the erosion profile is not affected. At $\sim$10,500 h, the thruster is returned to TH 15, but the keeper orifice was eroded to twice its initial diameter. Although the DCA flow rate is increased upon returning to TH 15, the keeper orifice is larger and so the neutral number density does not return to the pre-TH-8 value. Because of the enlarged orifice and corresponding reduced density, the orifice cannot protect itself with CEX collisions and erosion continues with the TH-8 profile even though the thruster is operating at TH 15. This erosion profile remains the same throughout the remainder of the ELT, eventually eroding away the entire keeper faceplate.

Acknowledgments

References

[1] Sovey, J. S., "Improved Ion Containment Using a Ring-Cusp Ion thruster," *Journal of Spacecraft and Rockets*, Vol. 21, No. 5, Sept.–Oct. 1984, pp. 488–495.

[2] Anderson, J. R., Goodfellow, K., Polk, J. E., Rawlin, V. K., and Sovey, J. S., "Performance Characteristics of the NSTAR Ion Thruster During an On-Going Long Duration Ground Test," *IEEE Aerospace Conference*, Vol. 4, Inst. of Electronics and Electrical Engineers, Big Sky, MT, 18–25 Mar. 2000, pp. 99–122.

[3] Anderson, J. R., Goodfellow, K., Polk, J. E., Shotwell, R. F., Rawlin, V. K., Sovey, J. S., and Patterson, M. J., "Results of an On-Going Long Duration Ground Test of the DS1 Flight Spare Ion Engine," 35th Joint Propulsion Conference, Los Angeles, AIAA Paper 99-2857, 20–24 June 1999.

[4] Patterson, M. J., Rawlin, V. K., Sovey, J. S., Kussmaul, M. J., and Parkes, J., "2.3 kW Ion Thruster Wear Test," 31st Joint Propulsion Conference, San Diego, CA, AIAA Paper 95-2516, 10–12 July 1995.

[5] Polk, J. E., Anderson, J. R., Brophy, J. R., Rawlin, V. K., Patterson, M. J., and Sovey, J. S., "The Effect of Engine Wear on Performance in the NSTAR 8000 Hour Ion Engine Endurance Test," 33rd Joint Propulsion Conference, Seattle, WA, AIAA Paper 97-3387, 6–9 July 1997.

[6] Polk, J. E., Anderson, J. R., Brophy, J. R., Rawlin, V. K., Patterson, M. J., Sovey, J. S., and Hamley, J., "An Overview of the Results from an 8200 Hour Wear Test of the NSTAR Ion Thruster," 35th Joint Propulsion Conference, Los Angeles, AIAA Paper 99-2446, 20–24 June 1999.

[7] Polk, J. E., Patterson, M. J., Brophy, J. R., Rawlin, V. K., Sovey, J. S., Myers, R. M., Blandino, J. J., Goodfellow, K., and Garner, C. E., "A 1000-Hour Wear Test of the NSTAR Ion Thruster," 32nd Joint Propulsion Conference, Lake Buena Vista, FL, AIAA Paper 96-2717, 1–3 July 1996.

[8] Sengupta, A., Anderson, J. R., Brophy, J. R., Rawlin, V. K., and Sovey, J. S., "Performance Characteristics of the Deep Space 1 Flight Spare Ion Thruster Long Duration Test After 21,300 Hours of Operation," 38th Joint Propulsion Conference, Indianapolis, IN, AIAA Paper 2002-3959, 7–10 July 2002.

[9] Sengupta, A., Brophy, J. R., Anderson, J. R., Garner, C. E., de Groh, K., Karniotis, T., and Banks, B., "An Overview of the Results from the 30,000 Hr Life Test of Deep Space 1 Flight Spare Ion Engine," 40th Joint Propulsion Conference, Fort Lauderdale, FL, AIAA Paper 2004-3608, 11–14 July 2004.

[10] Sengupta, A., Brophy, J. R., and Goodfellow, K., "Status of the Extended Life Test of the Deep Space 1 Flight Spare Engine After 30,352 Hours of Operation," 39th Joint Propulsion Conference, Huntsville, AL, AIAA Paper 2003-4558, 20–23 July 2003.

[11] Kolasinski, R. D., and Polk, J. E., "Characterization of Cathode Keeper Wear by Surface Layer Activation," *Journal of Propulsion and Power*, Vol. 20, No. 6, Nov.–Dec. 2004, pp. 992–999.

[12] Herman, D. A., and Gallimore, A. D., "A High-Speed Axial Reciprocating Probe Positioning System for Interrogating the Discharge Plasma of a 30 cm Ion thruster," 38th Joint Propulsion Conference, Indianapolis, IN, AIAA Paper 2002-4256, 7–10 July 2002.

[13] Herman, D. A., and Gallimore, A. D., "Comparison of Discharge Plasma Parameters in a 30-cm NSTAR Type Ion Engine with and Without Beam Extraction," 39th Joint Propulsion Conference, Huntsville, AL, AIAA Paper 2003-5162, 20–23 July 2003.

[14] Herman, D. A., McFarlane, D. S., and Gallimore, A. D., "Discharge Plasma Parameters of a 30 cm Ion Thruster Measured Without Beam Extraction Using a High-Speed Axial Reciprocating Probe Positioning System," 28th International Electric Propulsion Conference, Toulouse, France, Electric Rocket Propulsion Society, Paper IEPC-03-0069, 17–21 Mar. 2003.

[15] Williams, G. J., "The Use of Laser-Induced Fluorescence to Characterize Discharge Cathode Erosion in a 30 cm Ring-Cusp Ion thruster," Ph.D. Thesis, Dept. of Aerospace Engineering, Univ. of Michigan, Ann Arbor, MI, 2000.

[16] Williams, G. J., Smith, T. B., and Gallimore, A. D., "30 cm Ion Thruster Discharge Cathode Erosion," 27th International Electric Propulsion Conference, Pasadena, CA, Electric Rocket Propulsion Society, Paper IEPC-01-306, 14–19 Oct. 2001.

[17] Williams, G. J., Smith, T. B., Hidaka, Y., and Gallimore, A. D., "FMT-2 Discharge Cathode Erosion Rate Measurements via Laser-Induced Fluorescence," 36th Joint Propulsion Conference, Huntsville, AL, AIAA Paper 2000-3663, 17–19 July 2000.

[18] Williams, G. J., Smith, T. B., Patrick, T. A., and Gallimore, A. D., "Characterization of the FMT-2 Discharge Cathode Plume," 26th International Electric Propulsion Conference, Kitakyushu, Japan, Electric Rocket Propulsion Society, Paper IEPC-99-104, Oct. 1999.

[19] Herman, D. A., "The Use of Electrostatic Probes to Characterize the Discharge Plasma Structure and Identify Discharge Cathode Erosion Mechanisms in Ring-Cusp Ion Thrusters," Doctoral Thesis, Dept. of Aerospace Engineering, Univ. of Michigan, Ann Arbor, MI, 2005.

[20] Herman, D. A., and Gallimore, A. D., "Near Discharge Cathode Assembly Plasma Potential Measurements in a 30-cm NSTAR-type Ion Engine Amidst Beam Extraction," 40th Joint Propulsion Conference, Fort Lauderdale, FL, AIAA Paper 2004-3958, 11–14 July 2004.

[21] Hershkowitz, N., "How Langmuir Probes Work," *Plasma Diagnostics*, edited by O. Auciello and D. L. Flamm, Academic Press, Boston, 1989, pp. 113–184.

[22] Hershkowitz, N., and Cho, M. H., "Measurement of Plasma Potential Using Collecting and Emitting Probes," *Journal of Vacuum Science and Technology A (Vacuum, Surfaces, and Films)*, Vol. 6, No. 3, May–June 1988, pp. 2054–2059.
doi:10.1116/1.575600

[23] Hershkowitz, N., Nelson, B., Pew, J., and Gates, D., "Self-Emissive Probes," *Review of Scientific Instruments*, Vol. 54, No. 1, Jan. 1983, pp. 29–34.
doi:10.1063/1.1137210

[24] Langmuir, I., "The Interaction of Electron and Positive Ion Space Charges in Cathode Sheaths," *Physical Review*, Vol. 33, June 1929, pp. 954–989.
doi:10.1103/PhysRev.33.954

[25] Mott-Smith, H. M., Langmuir, I., "The Theory of Collectors in Gaseous Discharges," *Physical Review*, Vol. 28, Oct. 1926, pp. 727–763.
doi:10.1103/PhysRev.28.727

[26] Laframboise, J. G., "Theory of Spherical and Cylindrical Langmuir Probes in a Collisionless, Maxwellian Plasma at Rest," Univ. of Toronto Inst. for Aerospace Studies, Rept. 100, Toronto, June 1966.

[27] Kameyama, I., and Wilbur, P. J., "Potential-Hill Model of High-Energy Ion Production Near High-Current Hollow Cathodes," 21st International Symposium on Space Technology and Science, Sonic City, Omiya, Japan, Japan Society for Aeronautical and Space Sciences Paper 98-a-2-17, 24–31 May 1998.

[28] Goebel, D. M., Jameson, K. K., Watkins, R. M., and Katz, I., "Hollow Cathode and Keeper-Region Plasma Measurements Using Ultra-Fast Miniature Scanning Probes," 40th Joint Propulsion Conference, Fort Lauderdale, FL, AIAA Paper 2004-3430, 11–14 July 2004.

[29] Jameson, K. K., Goebel, D. M., and Watkins, R. M., "Hollow Cathode and Keeper-Region Plasma Measurements," 41st Joint Propulsion Conference, Tucson, AZ, AIAA Paper 2005-3667, 10–13 July 2005.

[30] Jameson, K. K., Goebel, D. M., and Watkins, R. M., "Hollow Cathode and Thruster Discharge Chamber Plasma Measurements Using High-Speed Scanning Probes," 29th International Electric Propulsion Conference, Princeton, NJ, Electric Rocket Propulsion Society, Paper IEPC-2005-269, 31 Oct.–4 Nov. 2005.

[31] Coakley, P., and Hershkowitz, N., "Laboratory Double Layers," *Physics of Fluids*, Vol. 22, No. 6, June 1979, pp. 1171–1181.
doi:10.1063/1.862719

[32] Charles, C., and Boswell, R., "Current-Free Double-Layer Formation in a High-Density Helicon Discharge," *Applied Physics Letters*, Vol. 82, No. 9, Mar. 2003.

[33] Foster, J. E., and Patterson, M. J., "Plasma Emission Characteristics from a High Current Hollow Cathode in an Ion Thruster Discharge Chamber," 38th Joint Propulsion Conference, Indianapolis, IN, AIAA Paper 2002-4102, 7–10 July 2002.

[34] Doerner, R. P., Goebel, D. M., "Sputtering Yields of Ion Thruster Grid and Cathode Materials During Very Low Energy Xenon Plasma Bombardment," 39th Joint Propulsion Conference, Huntsville, AL, AIAA Paper 2003-4561, 20–23 July 2003.

[35] Doerner, R. P., Whyte, D. G., and Goebel, D. M., "Sputtering Yield Measurements during Low Energy Xenon Plasma Bombardment," *Journal of Applied Physics*, Vol. 93, No. 9, May 2003, pp. 5816–5823.
doi:10.1063/1.1566474

[36] Kolasinski, R. D., "Sputtering Yields of Ion Thruster Materials at Oblique Incidence," 40th Joint Propulsion Conference, Fort Lauderdale, FL, AIAA Paper 2004-4110, 11–14 July 2004.

[37] Yamamura, Y., "An Empirical Formula for Angular Dependence of Sputtering Yields," *Radiation Effects*, Vol. 80, Nos. 1–2, Feb. 1984, pp. 57–72.

doi:10.1080/00337578408222489

[38] Yamamura, Y., "Threshold Energies of Light-Ion Sputtering and Heavy-Ion Sputtering as a Function of Angle of Incidence," *Nuclear Instruments and Methods in Physics Research*, Vol. B2, 1984, pp. 627–630.

[39] Tartz, M., Manova, D., Neumann, H., Leiter, H., and Esch, J., "Sputter Investigation of Ion Thrusters Grid Materials," 41st Joint Propulsion Conference, Tucson, AZ, AIAA Paper 2005-4414, 10–13 July 2005.

[40] Cheney, K. B., and Pitkin, E. T., "Sputtering at Acute Incidence," *Journal of Applied Physics*, Vol. 36, No. 11, Nov. 1965, pp. 3542–3544.
doi:10.1063/1.1703035

[41] Wehner, G. K., "Influence of the Angle of Incidence on Sputtering Yields," *Journal of Applied Physics*, Vol. 30, No. 11, Nov. 1959, pp. 1762–1765.
doi:10.1063/1.1735051

[42] Duchemin, O. B., Brophy, J. R., Garner, C. E., Ray, P. K., Shutthanandan, V., and Mantenieks, M. A., "A Review of Low Energy Sputtering Theory and Experiments," 25th International Electric Propulsion Conference, Cleveland, OH, Electric Rocket Propulsion Society, Paper IEPC-97-068, 24–28 Aug. 1997.

[43] Sengupta, A., Brophy, J. R., and Goodfellow, K., "Wear Characteristics from the Extended Life Test of the DS1 Flight Spare Ion Thruster," 28th International Electric Propulsion Conference, Toulouse, France, Electric Rocket Propulsion Society, Paper IEPC-2003-026, 17–21 Mar. 2003.

[44] Garner, C. E., Sengupta, A., Kulleck, J. G., and Liu, T. M., "An Evaluation of the Discharge Chamber of the 30,000 Hr Life Test of the Deep Space 1 Flight Spare Ion Engine," 40th Joint Propulsion Conference, Fort Lauderdale, FL, AIAA Paper 2004-3609, 11–14 July 2004.

[45] Domonkos, M. T., Foster, J. E., and Patterson, M. J., "Investigation of Keeper Erosion in the NSTAR Ion Thruster," 27th International Electric Propulsion Conference, Pasadena, CA, Electric Rocket Propulsion Society, Paper IEPC-01-308, 15–19 Oct. 2001.

[46] Domonkos, M. T., Foster, C., and Soulas, G. C., "Wear Testing and Analysis of Ion Engine Discharge Cathode Keeper," *Journal of Propulsion and Power*, Vol. 21, No. 1, Jan.–Feb. 2005, pp. 102–110.

[47] Williams, G. J., Domonkos, M. T., and Chavez, J. M., "Measurement of Doubly Charged Ions in Ion Thruster Plumes," 27th International Electric Propulsion Conference, Pasadena, CA, Electric Rocket Propulsion Society, Paper IEPC-01-310, 15–19 Oct. 2001.

[48] Rovey, J. L., "A Multiple-Cathode, High-Power, Rectangular Ion Thruster Discharge Chamber for Increasing Thruster Lifetime," Ph.D. Thesis, Dept. of Aerospace Engineering, Univ. of Michigan, Ann Arbor, MI, 2006.

[49] Rovey, J. L., Herman, D. A., and Gallimore, A. D., "Potential Structure and Propellant Flow Rate Theory for Ion Thruster Discharge Cathode Erosion," 29th International Electric Propulsion Conference, Princeton, NJ, Electric Rocket Propulsion Society, Paper IEPC-2005-022, 31 Oct.–4 Nov. 2005.

[50] Kameyama, I., and Wilbur, P. J., "Effects of External Flow Near High-Current Hollow Cathodes on Ion-Energy Distributions," 25th International Electric Propulsion Conference, Cleveland, OH, Electric Rocket Propulsion Society, Paper IEPC-97-173, 24–28 Aug. 1997.

[51] Domonkos, M. T., "Evaluation of Low-Current Orificed Hollow Cathodes," Ph.D. Thesis, Dept. of Aerospace Engineering, Univ. of Michigan, Ann Arbor, MI, 1999.

[52] Boyd, I. D., Dressler, R. A., "Far Field Modeling of the Plasma Plume of a Hall Thruster," *Journal of Applied Physics*, Vol. 92, No. 4, Aug. 2002, pp. 1764–1774.
doi:10.1063/1.1492014

[53] Oh, D. Y., "Computational Modeling of Expanding Plasma Plumes in Space Using a PIC-DSMC Algorithm," Ph.D. Thesis, Dept. of Aeronautics and Astronautics, Massachusetts Inst. of Technology, Cambridge, MA, 1996.

E. Choueiri
Associate Editor